The Possibility of Determining Whether Organized Cloud Clusters Will Develop into Tropical Storms by Detecting Warm Core Structures from Advanced Microwave Sounding Unit Observations

Kotaro Bessho
Typhoon Research Department, Meteorological Research Institute,
Nagamine 1-1, Tsukuba 305-0052, Japan

Tetsuo Nakazawa,
Typhoon Research Department, Meteorological Research Institute,
Nagamine 1-1, Tsukuba 305-0052, Japan

Shuji Nishimura
Japan Meteorological Agency / Regional Specialized Meteorological Center Tokyo – Typhoon Center
1-3-4 Otemachi, Chiyoda-ku, Tokyo, Japan

Koji Kato
Japan Meteorological Agency / Meteorological Satellite Center
3-235 Nakakiyoto, Kiyose-shi, Tokyo, Japan

Abstract

The air temperature profiles of organized cloud clusters developing or not developing into tropical storms (TSs) over the western North Pacific in 2004 were investigated from Advanced Microwave Sounding Unit (AMSU) observations and the results of Dvorak analyses for the cloud clusters. First, typical temperature profiles of the clusters developing or not developing into TSs were compared. From this comparison, positive temperature anomalies in the upper troposphere were found in both clusters, while the values and spatial sizes of the anomalies for the clusters that developed into TS were larger than those for the ones that did not. Statistical analysis was then performed on the temperature anomalies near the center of all clusters retrieved from AMSU observational data. The average anomalies increased along with the intensity of the clusters indicated by the T-number, as estimated using the Dvorak technique. Time series analysis of temperature anomalies in the upper levels of the clusters was performed, and warm core structures were defined by the threshold derived from these anomalies. Using this definition, almost 70% of the clusters that had warm cores developed into TSs, while 85% of those that did not finally dissipated without such development. For the warm-core clusters that developed into TSs, the lead time from the detection of their warm core using AMSU observations to their recognition as TS was 27.7 hours. It is suggested that there is a strong possibility of detecting and forecasting the genesis of TSs using air temperature anomalies derived from AMSU data.

1. Introduction

Many cloud clusters form over the western North Pacific. Some of these are well organized, rotate cyclonically, and finally develop into tropical storms (TSs), although most dissipate without such development. Despite the importance of distinguishing whether clusters will turn into TSs in terms of marine warnings and tropical cyclone forecasting, it remains difficult to forecast tropical cyclone genesis using numerical models. For this reason, forecasters at tropical cyclone warning centers worldwide have relied operationally on the Dvorak technique to estimate the potential of clusters to develop into TSs (Dvorak 1975 and Dvorak 1984). This technique is based on subjective analysis, and is used as a tool for judging the formation of tropical cyclones and evaluating their intensity from values such as the central surface pressure and maximum wind speed using the patterns and features of clouds observed by visible and infrared imagers on satellites. The *Tropical number* (T-number) index is defined in the Dvorak technique to express the intensity of a tropical cyclone. T-numbers range from one to eight, and are counted in increments of 0.5. T-number 1 (T1) corresponds to the minimum level of tropical cyclone intensity, while T8 describes the maximum level.

The Dvorak technique has endured for more than 30 years, and has saved huge number of lives from tropical cyclones (Velden *et al*. 2006). While this technique is considered to be a de facto standard of satellite analysis for tropical cyclones, it is not without its limitations. First, it involves subjective analysis, and considerable training and experience are needed to master the technique. Second, it is difficult to estimate the intensity of tropical cyclones correctly in their genesis stage, especially when central dense overcasts cover the cyclonic circulation at low level. Tropical cyclones in the genesis stage are usually so small that they cannot be analyzed properly using the Dvorak method, especially when dealing with tropical cyclones formed from monsoon troughs in the western North Pacific. While an objective version of the Dvorak technique has been developed to overcome the first limitation (Velden *et al*. 1998), there is a strong need for a new approach to break the barriers represented by the genesis stage of tropical cyclones.

Recently, microwave sensors on board low-earth-orbit satellites have been significantly improved and enhanced, including microwave imagers, sounders and scatterometers. Among these, microwave imagers are used to fix the center of tropical cyclones and ascertain their structure (Hawkins *et al*. 2001 and Lee *et al*. 2002). They can detect microwave radiation from rain and ice particles through the dense clouds found in tropical cyclones. Using these characteristics of microwave imagers, Hoshino and Nakazawa (2007) presented an objective method of intensity estimation for tropical cyclones in the developing and mature stages. Microwave scatterometers can also estimate the sea surface wind distribution in and around tropical cyclones (Katsaros *et al*. 2001). By way of example, Sharp *et al*. (2002) and Gierach *et al*. (2007) inferred tropical cyclone genesis using the vorticity retrieved from observational data produced by the scatterometer of QuikSCAT. Unfortunately, however, occasions of QuikSCAT observation for one tropical cyclone are up to twice a day.

As a new generation of microwave sounders, Advanced Microwave Sounding Units (AMSUs) are now used to observe air temperature profiles within dense clouds at a more detailed level of spatial resolution than former sounders (Kidder *et al*. 2000). AMSUs are now employed on the NOAA-15, -16, -18 satellites, MetOp and the Earth Observing Satellite (EOS) Aqua. From the observations of five AMSUs, the air temperature structures of tropical cyclones can be sensed up to ten times a day. Moreover, warm core structures at the upper levels of tropical cyclones are retrieved from the temperature profiles observed by AMSUs. A warm core is defined as the center region of a tropical cyclone where the air temperature is higher than that of the surrounding environment because of the latent heat released by active convection within the cyclone. Warm cores are generally observed in the developing or mature stages of tropical cyclones (Hawkins and Rubsame 1968; Hawkins and Imbembo 1976; Heymsfield *et al*. 2001; Halverson *et al*. 2006). Though some research mainly targeting the developing or mature stages of tropical cyclones has statistically related the signals of warm cores detected by AMSU observations to the tropical cyclone intensity (Brueske and Velden 2003; Demuth *et al*. 2004; Demuth *et al*. 2006), the situation regarding warm core structures at the genesis stage of tropical cyclones remains unclear. This leaves the possibility of complementing the Dvorak technique to judge the genesis of tropical cyclones more objectively by using AMSU observations.

In this study, the air temperature structures of cloud clusters, some of which developed into TSs while others did not, were investigated using the AMSUs on board NOAA-15 and -16 in 2004. Particular attention was focused on the amplitude of positive temperature anomalies at 200 - 300 hPa in the clusters, as such anomalies correspond to warm cores. This article will first present the typical warm core structures of cloud clusters before investigating the amplitude of temperature anomalies at the upper levels of clusters classified by their final stage. The warm core structure in the cluster will then be defined using the threshold of the temperature anomalies. Finally, from the statistical analysis results of the warm core structures in the clusters, we will discuss the possibility of distinguishing whether a cluster will develop into a tropical cyclone or not in terms of the existence of warm cores in the clusters.

2. Early stage Dvorak analysis

The Meteorological Satellite Center (MSC) of the Japan Meteorological Agency (JMA) routinely monitored Organized Cloud Clusters (OCCs) over the western North Pacific that had the potential to develop into TSs (defined in terms of Tsuchiya *et al.* (2001)), and logged their locations and T-numbers since 1999 at six-hourly intervals. This process is called early stage Dvorak analysis (EDA). EDA is a part of JMA's Dvorak analysis, and also depends on subjective judgment using observational data from geostationary satellites. We used data from the results of EDA in this study to classify OCCs by their final stage.

JMA classifies tropical cyclones over the western North Pacific ocean into four grades based on their maximum wind speed (MWS) as shown in Table 1; they are typhoon (TY, MWS of 64 kt or more), severe tropical storm (STS, MWS of 48 kt or more

Table 1 Classification of tropical cyclones by JMA

Type of Tropical Cyclones	Maximum Wind Speed (MWS)	Code
Low Pressure Area		L
Tropical Depression	34 kt > MWS	TD
Tropical Storm	48 kt > MWS $\geq$ 34 kt	TS
Severe Tropical Storm	64 kt > MWS $\geq$ 48 kt	STS
Typhoon	MWS $\geq$ 64 kt	T

and less than 64 kt), tropical storm (TS, MWS of 34 kt or more and less than 48 kt), and tropical depression (TD, MWS of 34 kt or less). JMA also names tropical cyclones with a MWS of 34 kt or more and issues gale warnings for them to marine users. EDA, which is employed to distinguish TDs from TSs, includes the two steps outlined below.

As the first step, analysts investigate the cloud cluster's Cloud System Center (CSC) to distinguish OCCs from other cloud clusters. In this paper, an OCC is defined as a cloud cluster with a CSC. According to Dvorak (1984), a CSC has at least one of the four features below (illustrated in Figure 1). To determine the CSC, analysts select the most suitable one of the following:

i) Dense, cold (-31 $^{\circ}$C or colder) overcast bands that show some curvature around a relatively warm area. They should curve at least one-fifth of the distance around a ten-degree logarithmic spiral. When visible observations are available, cirrus lines will indicate anticyclone shear across the expected CSC.

ii) Curved cirrus lines indicating a center of curvature within or near a dense, cold (-31 $^{\circ}$C or colder) overcast.

iii) Curved low cloud lines showing a center of curvature within two degrees of a cold (-31 $^{\circ}$C or colder) cloud mass.

iv) Cumulonimbus (Cb) clusters rotating cyclonically in animated images.

(×: CSC, ⊗ : dense overcast, ⟶ɔɔ⟶ɔ : curved cirrus line)
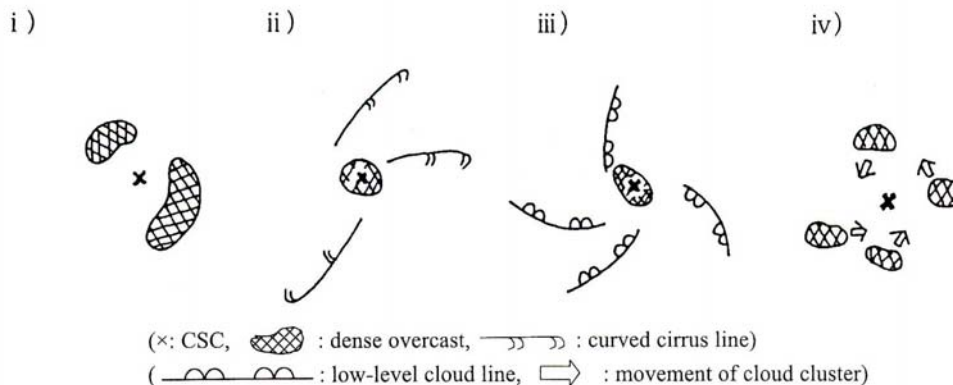(⟶∞⟶∞⟶ : low-level cloud line, ⟹ : movement of cloud cluster)

Figure 1 CSCs defined from four cloud patterns (i-iv) (after Tsuchiya *et al.* (2001))

After detecting the CSC, analysts give a T-number 1 (T1) diagnosis and judge the cyclogenesis as the second step of EDA. In this diagnosis, the T-number is determined as 1 when cloud systems have all five of the following conditions (Figure 2):

(1) The cloud clusters have persisted for 12 hours or more.

(2) The accuracy of estimation for the CSC in the clusters is 2.5° latitude or less.

(3) The CSC has persisted for six hours or more.

(4) The clusters have dense, cold (-31 $^{\circ}$C or colder) overcasts that appear less than 2° latitude from the CSC.

(5) The extent of the overcasts is more than 1.5° latitude.

An OCC is usually identified as a TD (not yet a TS) when the T-number becomes 1 or more, and is judged as a TS when the
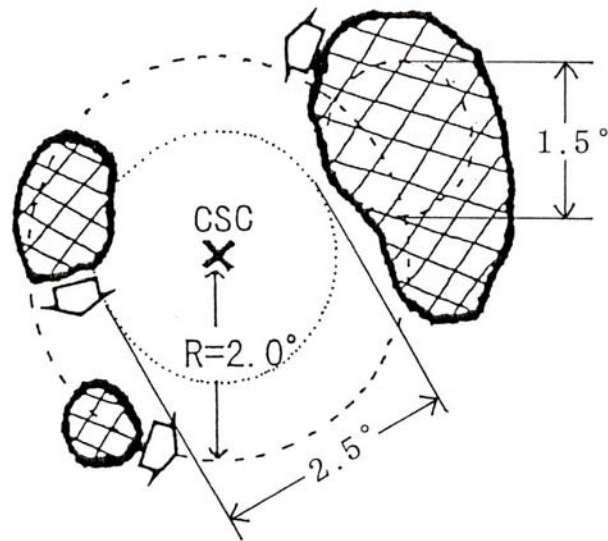

Figure 2 A conceptual model of cloud clusters satisfying T1. The shaded areas are dense, cold (-31 $^{\circ}$C or colder) overcasts. The estimation accuracy of the CSC is expressed by the dotted circle around it with a diameter of 2.5° (2). The broken circle with a radius of 2.0° indicates the region including the dense, cold overcast (4). The diameter of the circle drawn in the overcast on the right side of the CSC is 1.5°. This circle shows the size of the overcast (5). (after Tsuchiya *et al.* (2001))

MWS of the TD reaches 34 kt or more. On the other hand, an OCC with a T-number smaller than 1 is referred to as a low-pressure area (L) in EDA.

In this study, OCCs are classified by their final stage as follows: OCC_L are OCCs that stayed at the stage of L and finally dissipated; OCC_{TD} are OCCs that developed into TDs, but did not develop into TSs; OCC_{TS} are OCCs that developed into TSs.

3. Data

AMSU brightness temperature data from NOAA-15 and -16 in 2004 came courtesy of the Cooperative Institute for Research in the Atmosphere (CIRA) of Colorado State University (CSU). The air temperature profiles around OCCs were retrieved by a DDK algorithm developed by CIRA (Demuth *et al.* 2004 and Bessho *et al.* 2006). The retrieved temperature data on the footprint of AMSU were interpolated into a grid of 24° latitude by 24° longitude with a resolution of 0.2° centered on the CSC of OCCs after Barnes (1964). The retrieved air temperature data set had 30 pressure levels from 1000 to 10 hPa.

Air temperature anomalies were used for analysis of the warm core structure in OCCs. To calculate the temperature anomalies, the mean air temperature in a rectangular frame of 10° latitude by 10° longitude centered on the CSC of OCCs was subtracted from the air temperature at

each pressure level, which is almost the same as the method used by Knaff *et al*. (2004).

The EDA log file for 2004 lists 100 OCCs in the western North Pacific. Among them, 29 were $OCC_{TS,}$ 14 were OCC_{TD}, and the others were OCC_L. Eliminating the six cases with no AMSU observational data, 28 cases of OCC_{TS}, 13 cases of OCC_{TD} and 53 cases of OCC_L were used in this study. As the number of OCC_{TD} is too small to compare with those of OCC_L or OCC_{TS}, this study will mainly show the results of comparison between OCC_L and OCC_{TS}.

4. Examples of warm core structures of OCCs estimated from AMSU

The typical warm core structures of two OCCs are shown here before presenting the statistics of the air temperature anomalies retrieved from AMSU within OCCs. One OCC is numbered as 0428 (referred to below as EDA0428), and the other is as 0453 (EDA0453). EDA0428, which was an OCC_L, was detected as an OCC at 18Z on 3 June 2004 at 8.2^o N and 151.4^o E, and dissipated at 06Z on 4 June after a lifetime of just 12 hours. On the other hand, EDA0453, an OCC_{TS}, was first detected as an OCC at 06Z on 13 August 2004 at 13.2^o N and 144.4^o E. It reached T-number 1 at 00Z on 14 August at 14.5^o N and 140.5^o E and became a TD. It finally developed into a TS at 06Z on 16 August at 18.8^o N and 130.8^o E, and was named Typhoon Megi. JMA numbered this typhoon 0415.

Figure 3 shows Geostationary Operational Environmental Satellite-9 (GOES-9) infrared imagery and AMSU air temperature anomalies at the level of 200 hPa for EDA0428 at 21Z on 3 June and EDA0453 at 21Z on 13 August. At 21Z on 3 June, three hours had passed since EDA0428's genesis, whereas 15 hours had passed at 21Z on 13 August since EDA0453's detection as an OCC. It took two-and-a-half days to reach the stage of TS. While EDA0453 had very large and active convective clouds near its CSC, EDA0428 had scattered convective clouds near the center. Though both OCCs have positive temperature anomalies in the AMSU observational images, they look quite different. For EDA0453 of OCC_{TS}, the area of positive anomalies spreads widely corresponding to the large convective areas around its CSC, and the maximum temperature

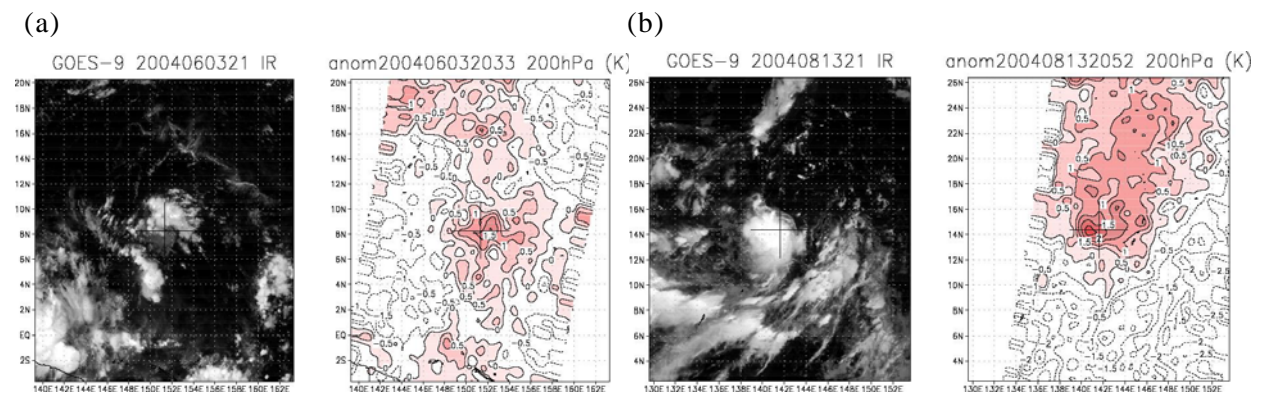(a)   (b)

Figure 3 Horizontal images of AMSU-retrieved temperature anomalies (K) at 200 hPa (right) and GOES-9 infrared brightness temperatures (left) for (a) EDA0428 at 21Z on 3 June, and (b) EDA0453 at 21Z on 13 August. The cross hairs in the images show the position of the CSC.
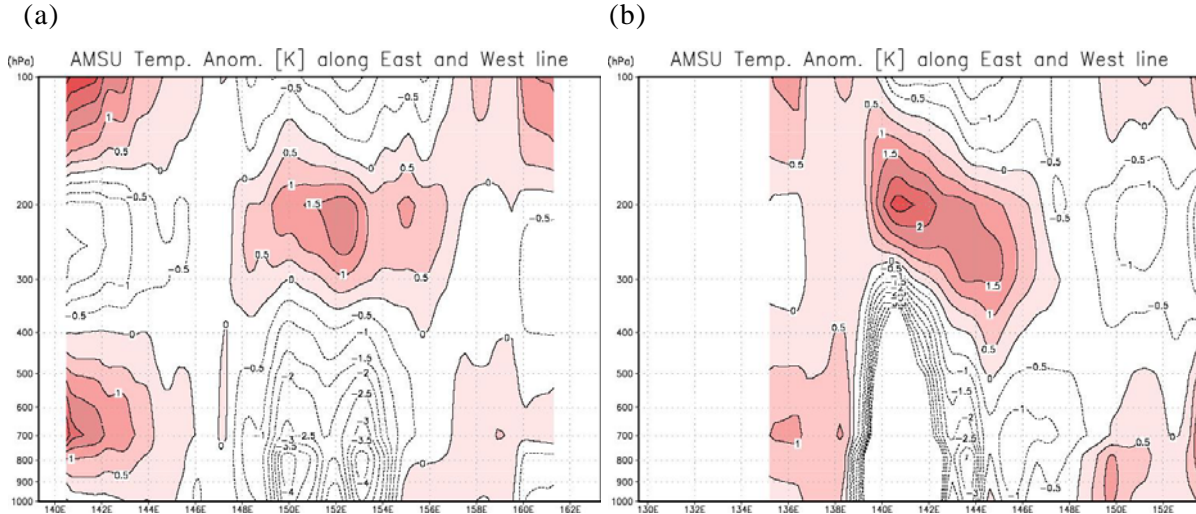
(a)　　　　　　　　　　　　　　　　　　　　(b)

Figure 4 Vertical cross sections of AMSU-retrieved temperature anomalies (K) along an east-to-west line through the CSC at the same observational time as Figure 3 for (a) EDA0428 and (b) EDA0453.

anomaly reached 2.5 K or more. In contrast, EDA0428 of OCC_L shows small regions of positive temperature anomalies and a maximum value of 1.5 K.

Figure 4 shows vertical cross sections of the air temperature anomalies in OCCs retrieved from AMSU data along an east-to-west line through the CSC at the same observational time as Figure 3. Note that retrieved air temperatures are not reliable near the center of OCCs below 300 hPa because of contamination from heavy rainfall. Both EDA0428 and EDA0453 have positive temperature anomalies near the center from 300 hPa to 150 hPa. While the peak temperature anomaly for EDA0428 is 1.5 K and is located at 250 - 200 hPa over the CSC, the peak for EDA0453 is 2.5 K or more, and is located at 200 hPa.

Figure 5 shows the pressure-time cross sections of air temperature anomalies of OCCs
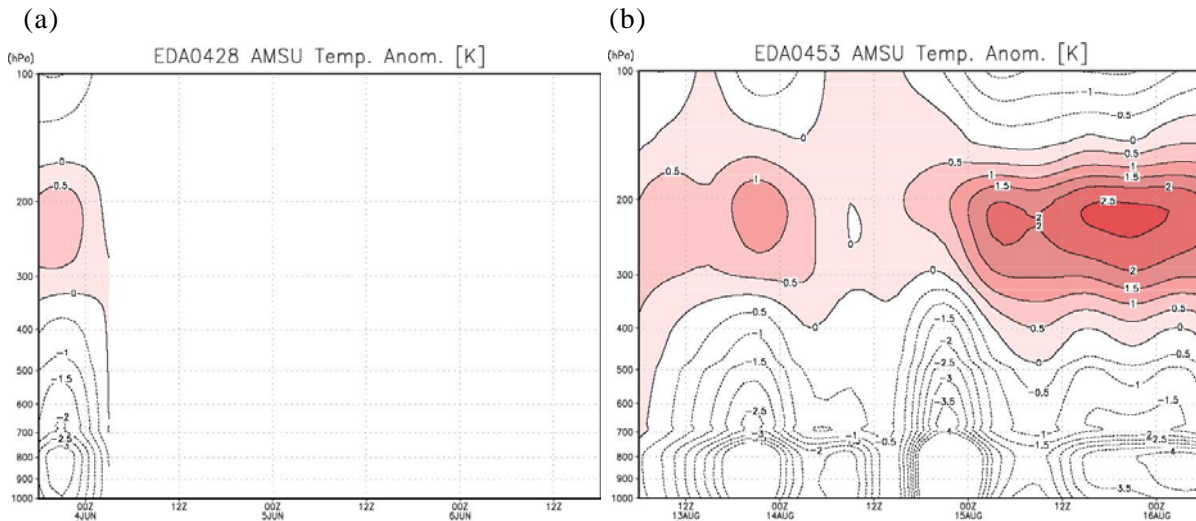
(a)　　　　　　　　　　　　　　　　　　　　(b)

Figure 5　Pressure-time cross sections of air temperature anomalies (K) averaged within a rectangle of 4° latitude by 4° longitude centered on the CSCs retrieved from AMSU observations in the cases of (a) EDA0428 and (b) EDA0453.

Table 2   Statistics of air temperature anomalies retrieved from AMSU within OCCs classified by their final stage and T-number at (a) 200 hPa, (b) 250 hPa and (c) 300 hPa. Statistically significant values at the 95% level are denoted by an asterisk.

(a)

200 hPa	Number of cases	T-number	Avg. anom. in 4° x 4°	Max. anom. in 10° x 10°	Fraction of anomalies more than 1 K in 4° x 4°
OCC_L	108	0.0	0.11 (0.48)*	2.06 (0.73)*	10.6 (16.0)*
OCC_{TD}	47	0.0	0.37 (0.50)	2.25 (0.70)*	18.7 (19.0)
	36	1.0	0.26 (0.45)	2.25 (0.76)*	14.0 (17.9)
	11	1.5	0.66 (0.71)	2.53 (1.24)	27.9 (27.0)
OCC_{TS}	76	0.0	0.39 (0.54)	2.22 (0.66)*	20.4 (21.5)
	76	1.0	0.56 (0.59)*	2.19 (0.75)*	28.3 (26.9)*
	29	1.5	0.72 (0.70)*	2.47 (0.80)*	36.1 (30.2)*
	28	2.0	0.93 (0.63)*	2.51 (0.87)*	42.9 (31.4)*

(b)

250 hPa	Number of cases	T-number	Avg. anom. in 4° x 4°	Max. anom. in 10° x 10°	Fraction of anomalies more than 1 K in 4° x 4°
OCC_L	108	0.0	0.05 (0.41)*	1.47 (0.47)*	3.9 (9.1)*
OCC_{TD}	47	0.0	0.31 (0.47)	1.54 (0.40)*	12.1 (19.0)
	36	1.0	0.28 (0.41)	1.70 (0.41)*	10.8 (16.4)
	11	1.5	0.59 (0.54)	1.71 (0.59)	22.3 (29.5)
OCC_{TS}	76	0.0	0.40 (0.48)	1.60 (0.43)*	17.3 (24.0)
	76	1.0	0.51 (0.53)*	1.54 (0.51)*	20.8 (26.9)
	29	1.5	0.67 (0.65)*	1.72 (0.67)*	30.3 (34.3)*
	28	2.0	0.76 (0.58)*	1.74 (0.65)*	35.2 (34.4)*

(c)

300 hPa	Number of cases	T-number	Avg. anom. in 4° x 4°	Max. anom. in 10° x 10°	Fraction of anomalies more than 1 K in 4° x 4°
OCC_L	108	0.0	-0.02 (0.44)*	1.15 (0.45)*	2.4 (9.5)*
OCC_{TD}	47	0.0	0.15 (0.51)	1.28 (0.40)*	8.0 (18.2)
	36	1.0	0.23 (0.49)	1.39 (0.43)*	12.0 (23.9)
	11	1.5	0.37 (0.48)	1.43 (0.44)	20.2 (25.1)
OCC_{TS}	76	0.0	0.31 (0.44)	1.28 (0.41)*	10.8 (17.3)
	76	1.0	0.32 (0.48)	1.27 (0.43)*	11.8 (20.6)
	29	1.5	0.43 (0.62)*	1.37 (0.47)*	19.5 (26.9)*
	28	2.0	0.40 (0.65)	1.50 (0.54)	24.8 (27.1)*

average within a rectangle of 4° latitude by 4° longitude centered on the CSC. Though EDA0428 has positive anomalies between 300-200 hPa, the values were less than 1 K around 21Z on 3 June when the horizontal and vertical snapshots in Figures 3(a) and 4(a) were observed. On the other hand, the anomalies of EDA0453 are sometimes large and sometimes small. At 21Z on 13 August (the same time as Figures 3(b) and 4(b)), the anomalies peaked at more than 1 K before becoming weaker and then breaking the 1 K level again. From 12Z on 15 August, EDA0453 had anomalies of more than 2 K.

5. Statistics of air temperature anomalies at upper levels for each OCC case

In this section, the statistics of air temperature anomalies at 200 - 300 hPa for OCCs are

presented as Table 2, and are classified by their final stage and T-number. At 200 hPa, the temperature anomalies of OCC_{TS} averaged within a rectangle of 4° latitude by 4° longitude centered on the CSC increase along with their T-number (Table 2 (a)). When the T-number is 0.0, the average anomaly is 0.39 K. The anomaly shows a value of 0.56 K with a T-number of 1.0 at which OCCs reach the TD stage, and shows 0.72 K for a T-number of 1.5. The average temperature anomaly finally reached 0.93 K with a T-number of 2.0 and larger (corresponding to the stage of TS), which is more than twice the value at a T-number of 0.0. This increasing tendency of average temperature anomalies at 200 hPa near the center of OCCs with T-numbers is similar to those at 250 and 300 hPa (Table 2 (b) and (c)).

On the other hand, average maximums of air temperature anomalies at 200 hPa of OCC_{TS} within a rectangle of 10° latitude by 10° longitude centered on the CSC show almost constant values of 2.2 - 2.5 K, and average maximums of anomalies at 250 and 300 hPa of OCC_{TS} also have almost constant values of 1.5 - 1.7 K and 1.3 - 1.5 K respectively, which are smaller than the value at 200 hPa. Considering the percentages of grid numbers for air temperature anomalies of more than 1 K within a rectangle of 4° latitude by 4° longitude centered on the CSC at 200 hPa of OCC_{TS}, the fractions of the air temperatures increase from 20.4% with a T-number of 0.0 to 42.9% with a T-number of 2.0. This tendency is also found from the percentages of grid numbers at 250 and 300 hPa.

In Table 2, some values are statistically significant at the 95% level, while others are not. From these tables, however, it is roughly understood that average temperature anomalies and the percentages of grid numbers of temperature anomalies more than 1 K near the center of the OCCs demonstrate an upward trend along with their T-numbers. This means that most OCCs have positive temperature anomalies called *warm cores* at troposphere upper levels. It is also understood that OCCs with larger T-numbers usually have larger temperature anomaly values than those with smaller T-numbers. If OCCs have the same T-number of 0.0, the average OCC_{TS} temperature anomalies are larger than those of OCC_L. In contrast, the average maximum air temperature anomalies of OCCs have almost constant values for all T-numbers.

6. Time series of air temperature anomalies at upper levels for each OCC case

Time series graphs of the temperature anomalies at upper levels were drawn for each OCC case. The objective was to understand the tendency of air temperature anomalies calculated from AMSU data and to find the threshold value of the anomalies to distinguish OCCs that developed into TSs from those that did not.

Figure 6(a) shows a time series of the air temperature anomalies at 200 hPa averaged within a rectangle of 4° latitude by 4° longitude centered on the CSC for all cases of OCC_L. For all cases except one, all lines are located below 0.9 K, and at 200, 250 and 300 hPa, only three cases of OCC_L have temperature anomalies of more than 0.9 K in their lifetime. This means that the temperature anomalies did not reach 0.9 K in the other 50 OCC_L cases. Figures 6(b) and (c) show
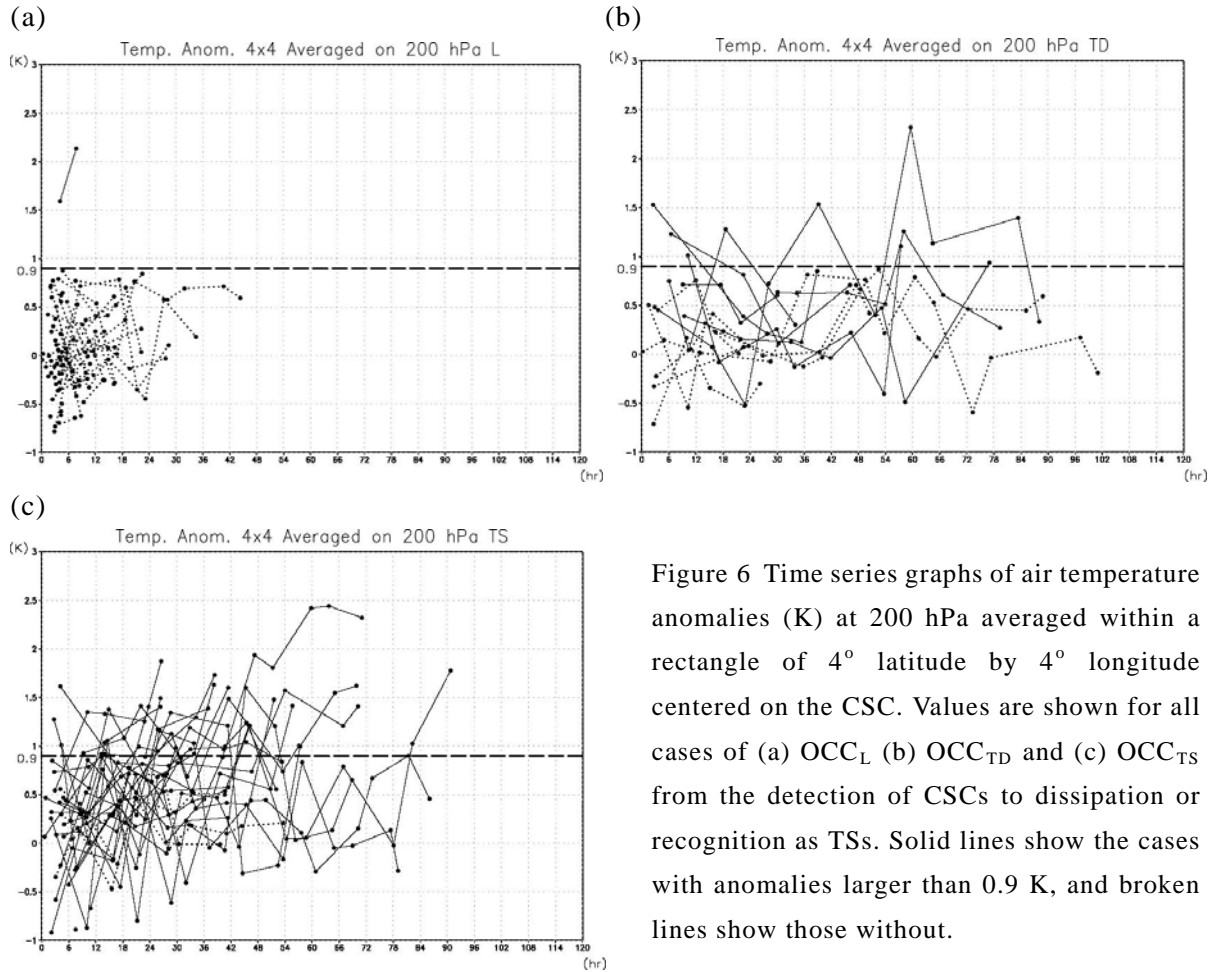
(a)

Temp. Anom. 4x4 Averaged on 200 hPa L

(b)

Temp. Anom. 4x4 Averaged on 200 hPa TD

(c)

Temp. Anom. 4x4 Averaged on 200 hPa TS

Figure 6 Time series graphs of air temperature anomalies (K) at 200 hPa averaged within a rectangle of 4° latitude by 4° longitude centered on the CSC. Values are shown for all cases of (a) OCC_L (b) OCC_{TD} and (c) OCC_{TS} from the detection of CSCs to dissipation or recognition as TSs. Solid lines show the cases with anomalies larger than 0.9 K, and broken lines show those without.

similar time series graphs of the temperature anomalies at 200 hPa for all cases of OCC_{TD} and OCC_{TS}. In most cases of OCC_{TS}, temperature anomalies become larger than 0.9 K at least once in their lifetime. For the cases of OCC_{TD}, almost half have anomalies larger than 0.9 K. From these observation results, we can conclude in this study that OCCs have a warm core structure at their upper levels when their air temperature anomalies (averaged within a rectangle of 4° latitude by 4° longitude centered on the CSC) exceed 0.9 K at 200, 250 or 300 hPa on one or more occasions in their lifetime.

Table 3 shows the number of OCCs classified by this definition, indicating that a total of 25 of 28 OCC_{TS} have warm core structures. On the other hand, 50 out of 53 OCC_L do not have a warm core. It is revealed that 89% of OCC_{TS} have a warm core at least once in their lifetime, while 94% of OCC_L do not. It is also clear that while almost 70% of all OCCs with a warm core structure developed to TS level, 85% of those with

Table 3 Numbers of each kind of OCC with or without warm core (WC) structures.

	With WC	Without WC	Total
OCC_L	3	50	53
OCC_{TD}	7	6	13
OCC_{TS}	25	3	28

no warm core stayed at the stage of L and dissipated. The threshold of 0.9 K as the definition of a warm core in the time series of upper temperature anomalies of OCCs is expected to be useful in distinguishing whether an OCC will develop into a TS.

7. Duration from detection of CSC to each stage in OCCs

For 25 cases of OCC_{TS} with a warm core, the average time from the detection of the CSC to evolution into a TS was 51.1 hours in 2004 (Figure

(a)

(b)

Figure 7 Schematic diagram of the average lifetime of (a) 25 cases of OCC_{TS} with a warm core and (b) 50 cases of OCC_L with no warm core. In the diagram, 'CSC' means the detection of the CSC, 'T1' represents the first judgment as T1, and 'TS' refers to the evolution of TS status.

7(a)). This means that the OCC_{TS} takes approximately two days to become a TS from the status of low-pressure area, and an average of 19.4 hours to reach the stage of T-number 1 (T1) for the first time from its appearance as an OCC. Meanwhile, the durations of 50 cases of OCC_L with no warm core from detection as an OCC to dissipation averaged only 14.0 hours (Figure 7(b)), which indicates that an OCC_L with no warm core structure usually dissipates in around half a day.

On the other hand, for OCC_{TS} with a warm core, the average time from detection as an OCC to the first recognition of their warm core structures in AMSU observations is 23.4 hours (Figure 8). This duration almost corresponds to the period from the appearance of an OCC to the first judgment of T1. For two cases of OCC_L with a warm core structure, the average time from detection as an OCC to the first recognition of a warm core structure was only 3.7 hours, and the average lifetime was 8 hours.

8. Discussion

Most previous studies on the structure and environmental field of tropical cyclones in the genesis stage in the western North Pacific have handled only cases of cloud clusters that developed to TS status (Briegel and Frank 1997; Ritchie and Holland 1999; Dickinson and Molinari 2002; Cheung 2004). This is because there was no official record for those that did not develop into TSs. Although such studies found important characteristics in the formation of tropical cyclones, most of these were *necessary conditions*. To reveal *sufficient conditions*, cloud clusters
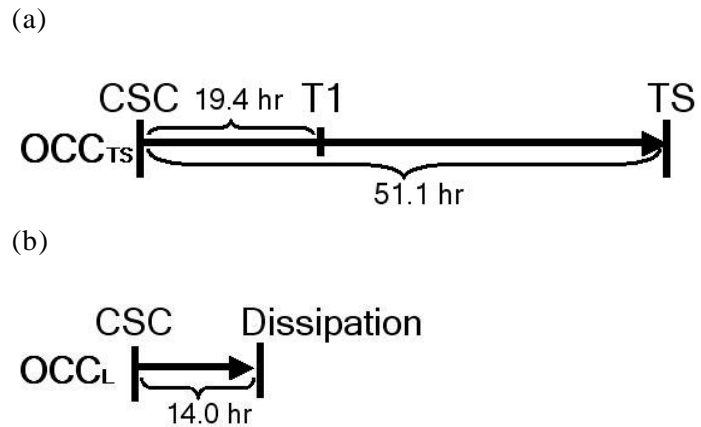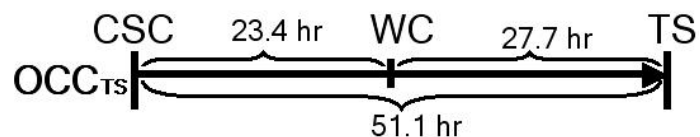

Figure 8 Schematic diagram of the average lifetime of 25 cases of OCC_{TS} with a warm core. In the diagram, the abbreviations are the same except for 'WC', which represents the first recognition of a warm core from AMSU observation.

that did not develop into TSs must be analyzed. Exceptions to these previous studies include works by CSU researchers published in the 1980s and 1990s (McBride and Zehr 1981; Lee 1989; Zehr 1992). In these papers, the authors used data obtained from soundings (McBride and Zehr 1981; Lee 1989), objective analysis (Zehr 1992) and satellite infrared imagery (Zehr 1992), and picked up many clusters that developed or did not develop into TSs in the western North Pacific. Our study also treats these clusters classified using EDA by MSC operationally. These EDA results include not only clusters with an intensity larger than that of TDs, but also tiny clusters at the start of rotation, which is a distinctive feature of our study. The analyses in this study were carried out using AMSU data representing the newest microwave sounding observations from low-earth-orbit satellites, which can detect warm core structures in cloud clusters directly. This is another advantage of the present paper compared with the earlier studies by CSU using the data of soundings, objective analyses and infrared imagery.

From Table 2, it was found that the average air temperature anomalies at the upper levels near the center of OCC_{TS} increase along with their T-numbers. On the other hand, the average maximum air temperature anomalies at the upper levels of OCC_{TS} keep almost constant values. The value at one grid point represents the air temperature within a rectangle of 0.2^{o} latitude by 0.2^{o} longitude in which there may be clear sky or many kinds of clouds, and the maximum air temperature anomaly of each OCC_{TS} is the value of one grid point extracted from all grid points in an observational area. It is clear that the average maximum temperature anomaly for all T-numbers has an almost constant value because the total amount of latent heat released from each convective cloud system included in one grid point has an upper limit. Meanwhile, the average temperature anomalies near the center of OCCs become larger with increased T-numbers. This phenomenon depends on the enlargement of the convective area within OCCs accompanying the increase of T-numbers. This is also understandable from the variation of fractions of temperature anomalies of more than 1 K near CSC of OCCs.

The percentage of grid points with anomalies of more than 1 K at 200 hPa of OCC_{L} with T-number of 0.0 is 10.6%. For OCC_{TS} with T-number of 0.0 at 200 hPa, the percentage is 20.4%, so it can be deduced that OCC_{TS} have double the convection area of OCC_{L}. Reflecting the difference between the percentages of grid points of anomalies more than 1 K in the two types of OCC, the average temperature anomalies of OCC_{TS} with T-number of 0.0 is 0.39 K, which is more than three times that of OCC_{L}. In EDA, OCCs need to satisfy the five conditions described in Section 2 to be diagnosed as T-number of 1.0. Both OCC_{L} and OCC_{TS} with T-number of 0.0 did not meet the requirements, but there is a distinct difference between their convective cloud system areas. It could be inferred that OCC_{TS} with T-number of 0.0 have some structural differences from OCC_{L} with T-number of 0.0. This presumption is another key to distinguishing OCC_{TS} from OCC_{L} at the stage of T-number of 0.0, but remains a future challenge.

The maximum temperature anomalies of OCC_{TS} with T-number of 1.0, which are significant at the 95% level, increase along with the height. The maximums are 1.27 K at 300 hPa,

1.54 K at 250 hPa, and 2.19 K at 200 hPa, and the same tendencies are also found from all classified OCC_S cases with T-numbers of 0.0 - 2.0. In previous observational studies, the heights of peak warm core anomalies vary from paper to paper, and differ from tropical cyclone to tropical cyclone. By way of example, the peak of the warm core in the intense Hurricane Hilda (1964) was located at 250 hPa (Hawkins and Rubsame 1968). On the other hand, the warming of Hurricane Erin (2001) was the greatest at 500 hPa (Halverson *et al*. 2006). In Knaff *et al*. (2004), it was found statistically that the peak of the warm core was located at the upper levels, and descended as the vertical wind shear increased for 186 tropical cyclone cases. They used air temperature information retrieved from AMSU brightness temperature data archived in CIRA, with a retrieval method same as that of this paper. The heights of warm core anomaly maximums are consistent between Knaff *et al*. (2004) and this paper because the same kinds of data set and retrieval method were used. However, there is a discrepancy between the height of the peak of 200 hPa in this paper (high) and that in other observational papers (low). The air temperatures at lower levels retrieved from AMSU data are cooler than normal, especially near the center of OCCs, due to the absorption and scattering of microwave radiation by liquid water and ice particles. This attenuation effect of microwaves could have brought lower maximum temperature anomalies at 300 hPa than those at 200 hPa.

In Zehr (1992), it was found that clusters developing into TSs have a stage of convective burst in their lifetime from genesis to emergence as a TS. Convective burst is a phenomenon of convection within clusters or tropical cyclones expressed by a peak of low infrared brightness temperature before appearance as a TSs. Once clusters experience convective burst, all the convections become active, and the phenomenon is usually found 24 hours before the incidence of tropical cyclones. In our study, temperature anomalies near the center of clusters at upper levels sometimes reach the peak before developing into tropical cyclones, as described in Figure 5(b). This appearance of a warm core structure within clusters at upper levels agrees with the convective burst in Zehr (1992). The convective burst is considered as the first occurrence of T-number 1 in EDA results, and has an average timing of 19.4 hours for the OCC_{TS} with a warm core in EDA files. The timing is almost the same as that of the first detection of a warm core in OCC_{TS} at an average of 23.4 hours. A possible scenario behind this is as follows: when the cluster has a convective burst in the infrared imagery, it is recognized as T-number 1. After a few hours, the convective burst provides large amounts of latent heat to the upper troposphere near the center of the cluster, and the warm core structure is observed by AMSU. This hypothesis must be proved by further studies.

As outlined in Chapter 7, the average period from the detection of the CSC of an OCC_{TS} to development into a TS is 51.1 hours (Figure 7(a)), and the period from the detection of the CSC in 25 cases of OCC_{TS} with warm cores to the first retrieval of the warm core is 23.4 hours (Figure 8). If the warm core retrieved from AMSU data is regarded as a sign of TS genesis, the lead-time to its genesis is 27.7 hours. This indicates that the detection of warm cores in OCCs is a very useful tool for finding and forecasting TS genesis.

On the other hand, there were three cases of OCC_{TS} in which no warm core structure was observed in the lifetime from detection of the CSC to evolution into TS, while three cases of OCC_L did have warm core structures. Among these OCC_L cases, one was a misdetection of a cold low as a tropical low in the EDA file. This phenomenon is the same as that reported by Knaff *et al*. (2000), who found that two cyclonic weather systems located in the South Pacific Ocean, despite their similar appearance in infrared imagery, had very different vertical thermal structures observed from AMSU. This study also confirmed that AMSU observation is useful in distinguishing cyclones with a warm core at upper levels from those with a cold core. Two of the three OCC_{TS} cases with no warm core structure did in fact have warm core structures located far from the lower vortexes. For OCC_{TD}, the total number of cases is small, but half of them had warm cores and half did not. These exceptions mean that 30% of OCCs with warm core structures did not develop into TSs, while 5% of OCCs with no warm core did develop to TS status. To improve the performance of determining whether OCCs will develop into TSs, it is necessary to add another screening method. One possible solution for this is to use the lifetime of the OCC from CSC detection to dissipation as L or to evolution into a TS. The average lifetime of an OCC_L with no warm core is 14.0 hours, and that of an OCC_{TS} is 51.1 hours. From the difference in these durations, it is expected that an OCC_L can be distinguished from an OCC_{TS} in conjunction with AMSU warm core detection.

From the above discussion, it can be concluded that there is a strong possibility of detecting and forecasting the formation of TSs from AMSU observations. However, it is still necessary to add more detailed analysis to develop an objective method of detecting and forecasting TS genesis by the retrieval of warm cores from AMSU data and the monitoring of OCC durations. EDA operation was transferred from MSC to the Regional Specialized Meteorological Center (RSMC) Tokyo - Typhoon Center operated by JMA in 2007. RSMC Tokyo has been running a follow-on project from the research outlined in this paper since 2007. Using the AMSU data available in near-real time at MSC, RSMC will validate the method proposed in this paper to distinguish OCCs that will develop into TSs from those that will not, and will try to use other parameters retrieved from the raw brightness temperatures of AMSU channel 7 with the cooperation of JMA/ Meteorological Research Institute. This testbed study was performed using operational EDA. The progress of further research will also be presented in the near future.

9. Summary

Because of the subjective nature of the Dvorak analysis technique, it is necessary to develop an objective method of estimating the intensity of OCCs and detecting the formation of TSs. To this end, we first applied AMSU observational data to the analysis of air temperature profiles within OCCs developing or not developing into TSs over the western North Pacific in 2004. The results of EDA performed by JMA/MSC were introduced to distinguish OCCs developing from those not developing into TSs in this process. Two typical cases of OCC_{TS} and

OCC_L were shown to compare their inner temperature profiles at the upper levels. The OCC_{TS} had larger values and a wider anomaly region than OCC_L, though both clusters had positive anomalies.

As the next step, the temperature anomalies at 200, 250 and 300 hPa near the center of each classified OCC were averaged. For the OCC_{TS}, the average positive anomalies increased along with the T-number estimated using EDA. This tendency was also found in the relationship between the percentages of grid numbers for anomalies of more than 1 K near the centers of the OCC_{TS}, and the average anomalies and the percentage showed peak values at 200 hPa for each T-number of 0.0 - 2.0. On the other hand, the average maximums of the OCC anomalies showed almost constant values for each T-number.

In time series analysis of the temperature anomalies, most OCC_{TS} showed a value of larger than 0.9 K at least once, whereas the anomalies for most OCC_L were below 0.9 K throughout their lifetime. From these analyses, we defined warm core structures within OCCs using an air temperature anomaly threshold of more than 0.9 K in this paper.

Under this definition, warm cores were found in most OCC_{TS} but not in most OCC_L, and 70% of the OCCs with warm cores developed into TSs, while 85% of those with no warm core dissipated without such development. For OCC_{TS} with a warm core, the time from the observation of the warm core by AMSU to identification as a TS was 27.7 hours, meaning that there is a lead time of almost one day in detecting the genesis of TSs. From these results, we can conclude that there is a strong possibility of forecasting cyclogenesis from AMSU observations.

References
Barnes, S. L., 1964: A technique for maximizing details in numerical weather ma analysis. *J. Appl. Meteor.*, **3**, 396-409.

Bessho, K., M. DeMaria and J. A. Knaff, 2006: Tropical cyclone wind retrievals from the Advanced Microwave Sounding Unit (AMSU): Application to surface wind analysis. *J. Appl. Meteor. Climatol*, **45,** 399-415.

Briegel, L. M., and W. M. Frank, 1997: Large-scale influences on tropical cyclogenesis in the western North Pacific. *Mon. Wea. Rev.,* **125,** 1397-1413.

Brueske K. F. and C. S. Velden, 2003: Satellite-based tropical cyclone intensity estimation using the NOAA-KLM series Advanced Microwave Sounding Unit (AMSU). *Mon. Wea. Rev.,* **131,** 687-697.

Cheung, K. K. W., 2004: Large-scale environmental parameters associated with tropical cyclone formations in the western North Pacific. *J. Climate*, **17**, 466-484.

Demuth, J. L., M. DeMaria, J. A. Knaff and T. H. Vonder Haar, 2004: Evaluation of Advanced Microwave Sounding Unit tropical-cyclone intensity and size estimation algorithms. *J. Appl. Meteor.*, **43**, 282-296.

Demuth, J. D., M. DeMaria, and J. A. Knaff, 2006: Improvement of Advanced Microwave Sounding Unit tropical cyclone intensity and size estimation algorithms. *J. Appl. Meteor.*

Climatol, **45,** 1573–1581.

Dickinson, M., and J. Molinari, 2002: Mixed Rossby–gravity waves and western Pacific tropical cyclogenesis. Part I: Synoptic evolution. *J. Atmos. Sci.,* **59,** 2183-2196.

Dvorak, V. F., 1975: Tropical cyclone intensity analysis and forecasting from satellite imagery. *Mon. Wea. Rev.*, **103**, 420-430.

Dvorak, V. F., 1984: Tropical cyclone intensity analysis using satellite data. *NOAA Tech. Rep. NESDIS* 11, Washington, DC, 47pp.

Gierach, M. M., M. A. Bourassa, P. Cunningham, J. J. O'Brien, and P. D. Reasor, 2007: Vorticity-based detection of tropical cyclogenesis. *J. Appl. Meteor. Climatol*, **46,** 1214–1229.

Halverson, J. B., J. Simpson, G. Heymsfield, H. Pierce, T. Hock and L. Ritchie, 2006: Warm core structure of Hurricane Erin diagnosed from high altitude dropsondes during CAMEX-4. *J. Atmos. Sci.*, **63**, 309-324.

Hawkins, H. F., and D. T. Rubsame, 1968: Hurricane Hilda, 1964 II. Structure and budgets of the hurricane on October 1, 1964. *Mon. Wea. Rev.,* **96,** 617–636.

Hawkins, H. F., and S. M. Imbembo, 1976: The structure of a small, intense Hurricane - Inez 1966. *Mon. Wea. Rev.,* **104,** 418–442.

Hawkins, J. D., T. F. Lee, J. Turk, C. Sampson, J. Kent, and K. Richardson, 2001: Real–time internet distribution of satellite products for tropical cyclone reconnaissance. *Bull. Amer. Meteor. Soc.*, **82**, 567–578.

Heymsfield, G. M., J. B. Halverson, J. Simpson, L. Tian, and T. P. Bui, 2001: ER-2 Doppler radar investigations of the eyewall of Hurricane Bonnie during the Convection and Moisture Experiment-3. *J. Appl. Meteor.,* **40,** 1310–1330.

Hoshino, S. and T. Nakazawa, 2007: Estimation of tropical cyclone's intensity using TRMM/TMI brightness temperature data. *J. Meteor. Soc. Japan*, **85**, 437-454.

Katsaros, K. B., E. B. Forde, P. Chang, and W. T. Liu, 2001: QuikSCAT's SeaWinds facilitates early identification of tropical depressions in 1999 hurricane season. *Geophys. Res. Lett.*, **28**, 1043-1046.

Kidder, S. Q., M. D. Goldberg, R. M. Zehr, M. DeMaria, J. F. W. Purdom, C. S. Velden, N. C. Grody, and S. J. Kusselson, 2000: Satellite analysis of tropical cyclones using the Advanced Microwave Sounding Unit (AMSU). *Bull. Amer. Meteor. Soc.*, **81**, 1241-1259.

Knaff, J. A., R. M. Zehr, M. D. Goldberg and S. Q. Kidder, 2000: An example of temperature structure differences in two cyclone systems derived from the Advanced Microwave Sounder Unit. *Wea. Forecasting*, **15**, 476–483.

Knaff, J. A., S. A. Seseske, M. DeMaria and J. L. Demuth, 2004: On the influences of vertical wind shear on symmetric tropical cyclone structure derived from AMSU. *Mon. Wea. Rev.*, **132**, 2503-2510.

Lee, C. C., 1989: Observational analysis of tropical cyclogenesis in the western North Pacific. Part I: Structural evolution of cloud clusters. *J. Atmos. Sci.,* **46,** 2580-2598.

Lee, T. F., F. J. Turk, J. Hawkins, and K. Richardson, 2002: Interpretation of TRMM TMI images of tropical cyclones. *Earth Interactions*, **6**,1-17.

McBride, J. L. and R. Zehr, 1981: Observational analysis of tropical cyclone formation. Part II: Comparison of non-developing versus developing systems. *J. Atmos. Sci.,* **38,** 1132-1151.

Ritchie, E. A., and G. J. Holland, 1999: Large-scale patterns associated with tropical cyclogenesis in the western Pacific. *Mon. Wea. Rev.,* **127,** 2027-2043.

Sharp, R. J., M. A. Bourassa and J. J. O'Brien, 2002: Early detection of tropical cyclones using Seawinds-derived vorticity. *Bull. Amer. Meteor. Soc.*, **83**, 879-889.

Tsuchiya, A., T. Mikawa and A. Kikuchi, 2001: Method of distinguishing between early stage cloud systems that develop into tropical storms and ones that do not. *Geophys. Mag. Series 2*, **4**, 49-59.

Velden, C. S., T. L. Olander and R. M. Zehr, 1998: Development of an objective scheme to estimate tropical cyclone intensity from digital geostationary satellite infrared imagery. *Wea. Forecasting*, **13**, 172-186.

Velden, C. S., B. Harper, F. Wells, J. L. Beven, R. M. Zehr, T. L. Olander, M. Mayfield, C. C. Guard, M. Lander, R. Edson, L. Avila, A. Burton, M. Turk, A. Kikuchi, A. Christian, P. Caroff and P. McCrone, 2006: The Dvorak tropical cyclone intensity estimation technique: a satellite-based method that has endured for over 30 years. *Bull. Amer. Meteor. Soc.*, **87**, 1195-1210.

Zehr, R. M., 1992: Tropical cyclogenesis in the Western North Pacific. *NOAA Tech. Rep. NESDIS 61*, Washington, DC, 181 pp.